# Ultrasonically assisted drilling: A finite-element model incorporating acoustic softening effects

**V A Phadnis[1], A Roy and V V Silberschmidt**

Wolfson School of Mechanical and Manufacturing Engineering, Loughborough University, Loughborough, LE11 3TU, UK

E-mail: v.a.phadnis@lboro.ac.uk

**Abstract.** Ultrasonically assisted drilling (UAD) is a novel machining technique suitable for drilling in hard-to-machine quasi-brittle materials such as carbon fibre reinforced polymer composites (CFRP). UAD has been shown to possess several advantages compared to conventional drilling (CD), including reduced thrust forces, diminished burr formation at drill exit and an overall improvement in roundness and surface finish of the drilled hole. Recently, our in-house experiments of UAD in CFRP composites demonstrated remarkable reductions in thrust-force and torque measurements (average force reductions in excess of 80%) when compared to CD with the same machining parameters. In this study, a 3D finite-element model of drilling in CFRP is developed. In order to model acoustic (ultrasonic) softening effects, a phenomenological model, which accounts for ultrasonically induced plastic strain, was implemented in ABAQUS/Explicit. The model also accounts for dynamic frictional effects, which also contribute to the overall improved machining characteristics in UAD. The model is validated with experimental findings, where an excellent correlation between the reduced thrust force and torque magnitude was achieved.

## 1. Introduction

Carbon fibre-reinforced polymer (CFRP) composites are widely used in aerospace and automobile industries and several other structural applications owing to their superior mechanical and physical properties. CFRPs outperform structural metals in durability, high strength-to-weight ratio, stiffness and density [1-4]. In spite of these advantages, machining CFRPs is cumbersome due to highly abrasive carbon fibres, low thermal conductivity of epoxy and a weak interfacial bond between reinforced fibres and matrix.

Typically, parts made of CFRP composite are manufactured to the required final shape, though machining cannot be avoided to enable assembly of individual components. Holes need to be drilled to facilitate riveting and bolting of machined components; to serve this purpose; conventional drilling (CD) methods are often adopted. Apart from poor geometric tolerance and surface finish, CD can initiate various damage modes in CFRPs such as matrix cracking, burr formation, interfacial de-bonding, delamination and fibre pull-out [1, 2, 5-7]. Consequently, the load-carrying capacity of

[1] Vaibhav A. Phadnis
Wolfson School of Mechanical and Manufacturing Engineering, Loughborough University, UK
Tel :+44 (0) 1509 227634; Email : v.a.phadnis@lboro.ac.uk

Content from this work may be used under the terms of the Creative Commons Attribution 3.0 licence. Any further distribution of this work must maintain attribution to the author(s) and the title of the work, journal citation and DOI.
Published under licence by IOP Publishing Ltd

composite structure is affected. Additionally, rapid tool wear is caused by abrasive carbon fibres resulting in frequent tool replacement. To overcome these issues, a less intrusive drilling technique is needed.

Ultrasonically Assisted Drilling (UAD) is a hybrid machining technique, which has been used to improve machining of conventional metals and advanced composites in the recent past [5-12]. In UAD, high-frequency (typically in excess of 20 kHz) vibrations generated by a piezoelectric transducer are superimposed on a rotating standard twist drill bit in the axial direction, to enhance the cutting process [8, 11]. There are several advantages of UAD over CD such as reduction in drilling forces and torque, better surface finish, low tool wear and elimination/reduction in burr formation [11-13]. In CFRP, drilling forces have a direct effect on damage induced in composites. Hence it is considered to be the primary parameter affecting quality of a drilled hole [4, 7, 9]. Several studies performed over the last few years [10-12] indicate that vibrating a drill bit in the axial direction yields the maximum reduction in drilling-induced damage. In the experimental study conducted by Hochen and Hsu [13] it was concluded that ultrasonic machining have viable advantages over conventional machining processes, though, a slurry-based method was used instead of external exciting the conventional drill bit for hole making in CFRP. Wang [14] performed several experiments involving UAD in CFRP. Using a vibration frequency of 300 Hz to excite a high-speed-steel (HSS) and carbide drill bits of 0.5 mm diameter; it was observed that thrust forces were reduced relative to those in CD. Babitsky and Astashev [8, 11] reported that in UAD, hardly any axial thrust force reduction was seen whilst exciting drill bits in torsional mode, though considerable reduction in the drilling force was observed when the drill was vibrated in axial direction.

Very few researchers have attempted to model a UAD process using a finite-element (FE) technique due to the complexity involved in modelling of such processes and the extent of computational resources required, though analytical model [see e.g.14] to calculate thrust forces in UAD can be found. This paper presents development of a FE model of UAD in CFRP composite using general purpose software - Abaqus 6.11. The experimental results from our previous work are presented for validation purposes.

## 2. FE model of UAD in CFRP

### *2.1. Background and assumptions*

UAD includes superposition of ultrasonic vibrations onto the relative cutting motion between a drill bit and the workpiece drilled. This collective effect results in the substantial reduction in the drilling forces and torque [5-11]. Based on the preliminary observations from our UAD experiments [5-7], a CFRP workpiece undergoes plastic deformation under the influence of ultrasonic vibrations, the extent of which depends on the intensity of vibrations, resulting in softening the workpiece in the process zone. Additionally, surface temperature of the CFRP workpiece often exceeded glass- transition temperature of thermoset epoxy polymer matrix (170 - $190^0$ C), resulting in matrix burning. The reduced thrust force and torque observed in UAD is claimed to be due to the combined influence of ultrasonic vibrations giving rise to vibro-impact and localised heating phenomena. In this context, we define ultrasonic softening as, the phenomenon in which ultrasonic vibrations reduce the apparent static stress necessary for material to undergo permanent inelastic deformation.

In this work, a parametric modelling approach was used to account for acoustic (ultrasonic) and thermal softening phenomena during inelastic deformation of the CFRP workpiece. The behaviour of CFRP laminate in elastic regime was defined using the Hill's [16, 17] potential theory for anisotropic materials together with the rate-independent plasticity criterion incorporating effects of ultrasonic softening. An element-removal scheme was used based on the shear damage-initiation criterion to replicate the hole-making process. The temperature rise due to plastic straining was modelled assuming adiabatic conditions. It should be noted that the temperature is a plastic strain work conjugate in the adiabatic system; hence an element was also removed from the mesh when instantaneous temperature reaches the glass transition limit of the epoxy matrix (irrespective of

instantaneous plastic strain reaching the fracture strain), thus effectively softening the material at macroscale.

The primary assumptions of this material model are:

a. Instantaneous intensity of ultrasonic vibrations is proportional to plastic strain induced in CFRP laminate. This instantaneous ultrasonic intensity is defined in terms of ultrasonic energy per unit time transferred to the workpiece and is a function of instantaneous contact pressure between the drill bit and the workpiece, the frequency and amplitude of vibration.
b. The strain-rate dependence of CFRP laminate, especially in transverse and through-thickness directions, is small enough to be neglected owing to a low loading rate [6-8].
c. The temperature rise in CFRP laminate during its interaction with the vibrating drill tip is mainly due to plastic strain developed locally.

*2.2. Constitutive material model*

The workpiece material used in this study was commerciality available M21/T700 quasi-isotropic laminate of thickness 10 mm with individual ply thickness of 0.25 mm. Details of the material properties used in this simulations can be found Phadnis *et al.* [7]. The thermo-mechanical plasticity model proposed in this work is based on the quadratic yield criterion for anisotropic materials by Hill [16, 17] and non-linear isotropic hardening rule for rate-independent plasticity. The constitutive equations of this model for uniaxial loading are as follows:

The total strain tensor during deformation is the sum of elastic strain tensor and plastic strain tensor, given by

$$\boldsymbol{\varepsilon} = \boldsymbol{\varepsilon}^{\mathbf{el}} + \boldsymbol{\varepsilon}^{\mathbf{pl}}. \tag{1.1}$$

The elastic part of stresses is computed using a constitutive stress-strain relationship;

$$\boldsymbol{\sigma} = \mathbf{C} \,.\, \boldsymbol{\varepsilon} = (\boldsymbol{\varepsilon}^{\mathbf{el}} - \boldsymbol{\varepsilon}^{\mathbf{pl}}), \tag{1.2}$$

where, $\boldsymbol{\sigma}$ and $\boldsymbol{\varepsilon}$ are the second-order elastic stress and strain tensors while $\mathbf{C}$ is the fourth-order stiffness tensor. The yield function [16] for orthotropic CFRP material in rectangular Cartesian stress components is given by

$$\begin{aligned} f(\boldsymbol{\sigma}) &= \sqrt{F(\bar{\sigma}_{22}-\bar{\sigma}_{33})^2 + G(\bar{\sigma}_{33}-\bar{\sigma}_{11})^2 + H(\bar{\sigma}_{11}-\bar{\sigma}_{22})^2 + 2L\bar{\sigma}_{23}{}^2 + 2M\bar{\sigma}_{31}{}^2 + 2N\bar{\sigma}_{12}} \\ &= \left|\boldsymbol{\sigma}^{\mathbf{y}}\right| + R, \end{aligned} \tag{1.3}$$

where, *F, G, L, M, and N* are constants obtained from a set of the following equations.

$$\begin{aligned} F &= \frac{(\sigma^0)^2}{2}\left(\frac{1}{\bar{\sigma}_{33}^2}+\frac{1}{\bar{\sigma}_{11}^2}+\frac{1}{\bar{\sigma}_{22}^2}\right) = \frac{1}{2}\left(\frac{1}{R_{33}^2}+\frac{1}{R_{11}^2}+\frac{1}{R_{22}^2}\right), \qquad L = \frac{3}{2}\left(\frac{\tau^0}{\bar{\sigma}_{23}}\right)^2 = \frac{3}{2R_{23}{}^2} \\ G &= \frac{(\sigma^0)^2}{2}\left(\frac{1}{\bar{\sigma}_{22}^2}+\frac{1}{\bar{\sigma}_{33}^2}+\frac{1}{\bar{\sigma}_{11}^2}\right) = \frac{1}{2}\left(\frac{1}{R_{22}^2}+\frac{1}{R_{33}^2}+\frac{1}{R_{11}^2}\right) \qquad M = \frac{3}{2}\left(\frac{\tau^0}{\bar{\sigma}_{13}}\right)^2 = \frac{3}{2R_{13}{}^2} \\ H &= \frac{(\sigma^0)^2}{2}\left(\frac{1}{\bar{\sigma}_{11}^2}+\frac{1}{\bar{\sigma}_{22}^2}+\frac{1}{\bar{\sigma}_{33}^2}\right) = \frac{1}{2}\left(\frac{1}{R_{11}^2}+\frac{1}{R_{22}^2}+\frac{1}{R_{33}^2}\right) \qquad N = \frac{3}{2}\left(\frac{\tau^0}{\bar{\sigma}_{12}}\right)^2 = \frac{3}{2R_{12}{}^2} \end{aligned} \tag{1.4}$$

Here $\bar{\sigma}$ is the measured yield stress when applied as the only non-zero stress component, $\sigma^0$ is the initial yield stress and is $\tau^0$ the shear stress at yield such that, $\tau^0 = \sigma^0 / \sqrt{3}$. $R_{ij}$ are anisotropic yield

ratios and can be calculated from the CFRP yield strengths. $\sigma^y$ is the size of an initial yield surface, while $R$ is the isotropic hardening term:

$$R = \sigma^0(\boldsymbol{\varepsilon}^{\mathbf{pl}}, \dot{\theta}). \tag{1.5}$$

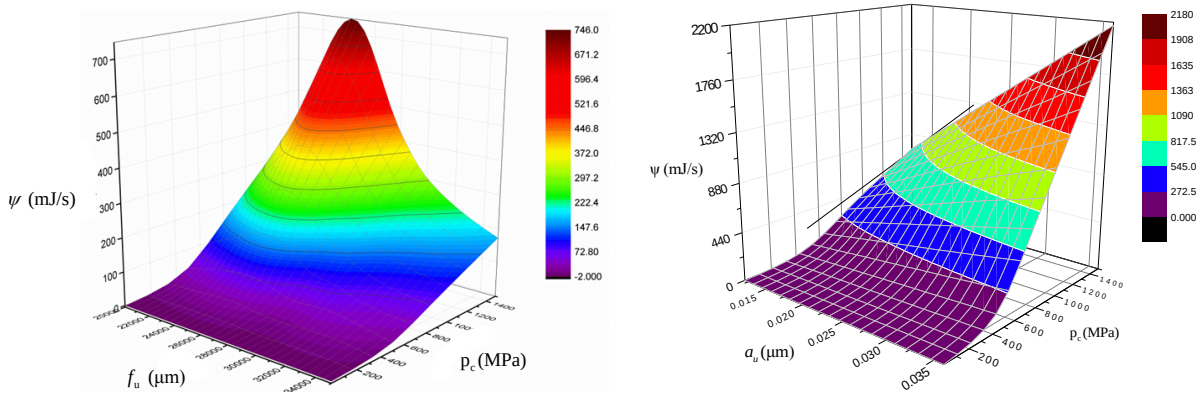
Plastic strain during deformation is defined as

$$\boldsymbol{\varepsilon}^{\mathbf{pl}} = D\left(\frac{\bar{\sigma}}{\sigma^0} - 1\right), \text{ for } \bar{\sigma} \geq \sigma^0 \tag{1.6}$$

where $\bar{\sigma}$, $\sigma^0$, $\boldsymbol{\varepsilon}^{\mathbf{pl}}$, and $D$ are yield stress at non-zero plastic stress, static yield stress, plastic strain and softening parameter respectively. $D$ is defined as, $D = D(\psi, \dot{\theta})$ where $\psi$ is ultrasonic energy per unit time and $\dot{\theta}$ is the temperature gradient due to work done towards plastic straining in an adiabatic system. It should be noted that ultrasonic energy per unit time, $\psi$ transmitted to the CFRP surface in the immediate contact with the drill tip is defined as

$$\psi = p_c . f_u . a_u . A_c \tag{1.7}$$

where $p_c$ is the instantaneous contact pressure exerted by the drill tip on the CFRP surface, $f_u$ and $a_u$ are the frequency and amplitude of ultrasonic vibration respectively. The magnitude of $\psi$ was calculated using (1.8) for the feed rate of 8 mm/min and spindle speed of 40 rpm. The area of contact and corresponding contact pressure was obtained through a number of simulations. The effect of a range of frequency and amplitude of ultrasonic vibration on the magnitude of ultrasonic energy per unit time is shown in Fig. 1a and b respectively.




(a) (b)

**Figure 1**. (a) Effect of $f_u$ on $\psi$ (Drill feed 8 mm/min, spindle speed 40 rpm, amplitude of vibration 12 μm peak-to-peak). (b) Effect of $a_u$ on $\psi$ (Drill feed 8 mm/min, spindle speed 40 rpm, frequency of vibration 25 kHz)

*2.3. Adiabatic heat transfer*

Heat generation caused by mechanical work associated with plastic straining was modelled in an adiabatic system. The ultrasonic frequency used in these simulations was 27.8 kHz resulting in rapid accumulation of ultrasonic energy in a highly localised regime in a very short period of time. Hence it was assumed that inelastic deformation due to plastic straining occurs so rapidly that heat had hardly

any time to diffuse through, and, thus, adiabatic analysis was sufficient to model the temperature rise in this local regime. The model assumed that plastic straining gives rise to a heat flux per unit volume, $r^{pl}$ such that;

$$r^{pl} = \eta\sigma : \dot{\varepsilon}^{pl}, \tag{1.8}$$

where $\eta$ is the constant inelastic heat coefficient, $\sigma$ is the instantaneous stress state and $\dot{\varepsilon}^{pl}$ is the plastic strain rate.

*2.4. Element removal scheme*

A hole-generation process in simulations of UAD was accomplished with the help of the element removal scheme in Abaqus/Explicit [19]. This scheme was based on the fracture mechanism initiated by shear damage and damage evolution linked to the energy dissipation during degradation of material's stiffness. The in-built Abaqus [19] shear damage-criterion utilised here is a phenomenological model for predicting the onset of damage due to shear-band localisation. It assumes that the equivalent plastic strain at the onset of damage $\tilde{\varepsilon}_s^{pl}$ is a function of the shear stress ratio and instantaneous plastic strain such that:

$$\tilde{\varepsilon}_s^{pl} = \tilde{\varepsilon}_s^{pl}(\chi_S, \tilde{\varepsilon}^{pl}), \tag{1.9}$$

where $\chi_S$ is a shear stress ratio:

$$\chi_S = \frac{\tau_S}{\tau_{\max}}. \tag{1.10}$$

Here $\tau_S$ is the total accumulated shear stress at the integration point of an element and $\tau_{\max}$ is the corresponding maximum shear stress. The criterion for damage initiation is met when the following condition is satisfied:

$$\omega_s = \int \left( \frac{1}{\boldsymbol{\varepsilon}_{\mathbf{S}}^{\mathbf{pl}}(\chi_S, \boldsymbol{\varepsilon}^{\mathbf{pl}})} \right). d\left(\boldsymbol{\varepsilon}^{\mathbf{pl}}\right) = 1 , \tag{1.11}$$

where $\omega_s$ is a state variable that increases monotonically with plastic deformation proportional to the incremental variation in the equivalent plastic strain.

The characteristic stress-strain behaviour of a material under uni-axial loading that undergoes progressive damage is shown in Fig. 2. In case of the elastic-plastic material this damage can be decomposed into two parts; softening of the yield stress and degradation of the elastic modulus. The solid curve in Fig. 3 represents the damaged stress-strain response, whereas the dashed line represents the undamaged behaviour. $\sigma_{y0}$ and $\bar{\varepsilon}_0^{pl}$ are yield stress and equivalent plastic strain at the onset of damage, while $\bar{\varepsilon}_f^{pl}$ is the equivalent plastic strain at failure, also known as *fracture strain*.

When material undergoes damage, the stress-strain relationship fails to accurately present its behaviour because of a strong mesh dependency linked to the strain localisation. Hence a different approach is required to trace the strain softening branch of the stress-strain curve.

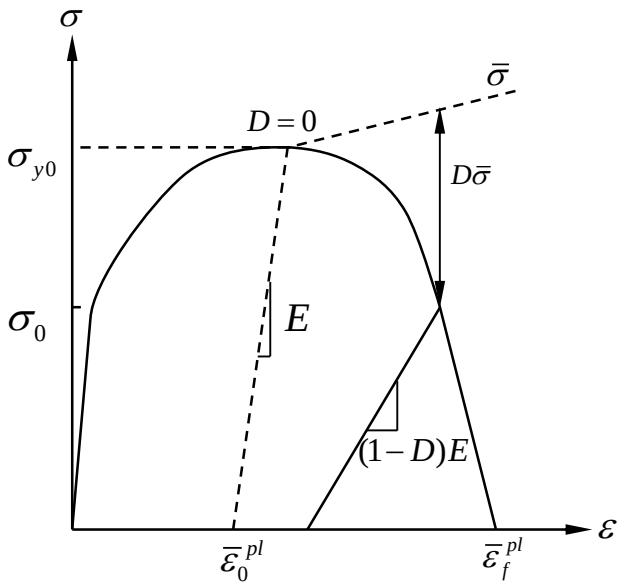



**Figure 2.** Stress-strain curve with progressive damage behaviour

Thus, Hillerborg's fracture energy approach [18] was employed in this model, which eventually helped to reduce mesh dependency by formulating a stress-displacement response after damage initiation. The fracture energy was idealised as work required to open a unit area of a crack, and expressed as:

$$G_f = \int_0^{u_{pl}^f} \sigma_y \, . \, d\left(\bar{u}^{pl}\right) , \tag{1.12}$$

where $\bar{u}^{pl}$ is the equivalent plastic displacement and can be considered as fracture energy conjugate of yield stress after the damage initiation: $\bar{u}^{pl} = 0$ at damage initiation and $\bar{u}^{pl} = L\bar{\varepsilon}^{pl}$ after it. Here $L$ is the characteristic length of an element in a meshed body that depends on its geometry and formulation. $D$ is the overall damage parameter : at damage initiation $D = 0,$ while at complete damage $D = 1$. The residual elastic modulus $E_r,$ after damage initiation can be calculated as,

$$E_r = (1 - D). E \ . \tag{1.13}$$

Evolution of the damage variable $\dot{d}$ associated with a relative plastic displacement was specified in a linear form as,

$$\dot{d} = \frac{\bar{u}^{pl}}{\bar{u}_f^{pl}} , \tag{1.14}$$

where $\bar{u}_f^{pl}$ is the equivalent plastic displacement at failure and can be calculated as

$$\bar{u}_f^{pl} = \frac{2G_f}{\sigma_{y0}} \tag{1.15}$$

*2.5. Contact and friction*

The contact and friction parameters used in the simulations were based on a number of experimental factors such as cutting speed, feed rate, drill geometry and surface properties. Contact between the twist drill and the CFRP laminate was defined by the general contact algorithm available in Abaqus/Explicit. This algorithm generated the contact forces based on the penalty-enforced contact method. A coefficient of dry friction at the interface between drill's cutting edge and laminate was assumed to be 0.03 based on the work by Lucas *et al.* [15].

*2.6. FE model setup*

*2.6.1. Geometric modelling and boundary conditions*

A 3D geometry of 6 mm twist drill with a point angle of 118° and helix angle of 31° was modelled in Abaqus. The drill was modelled as a rigid body, and the inertia effect was accounted for. The mesh was optimized to reduce the computational cost without compromising accuracy. A mesh size of CFRP work piece was refined in the immediate vicinity of the drilled area to capture high stress gradients during the drilling process. Elements in the refined cylindrical zone were removed when the failure criterion was met during simulations using element deletion discussed in section 2.4.

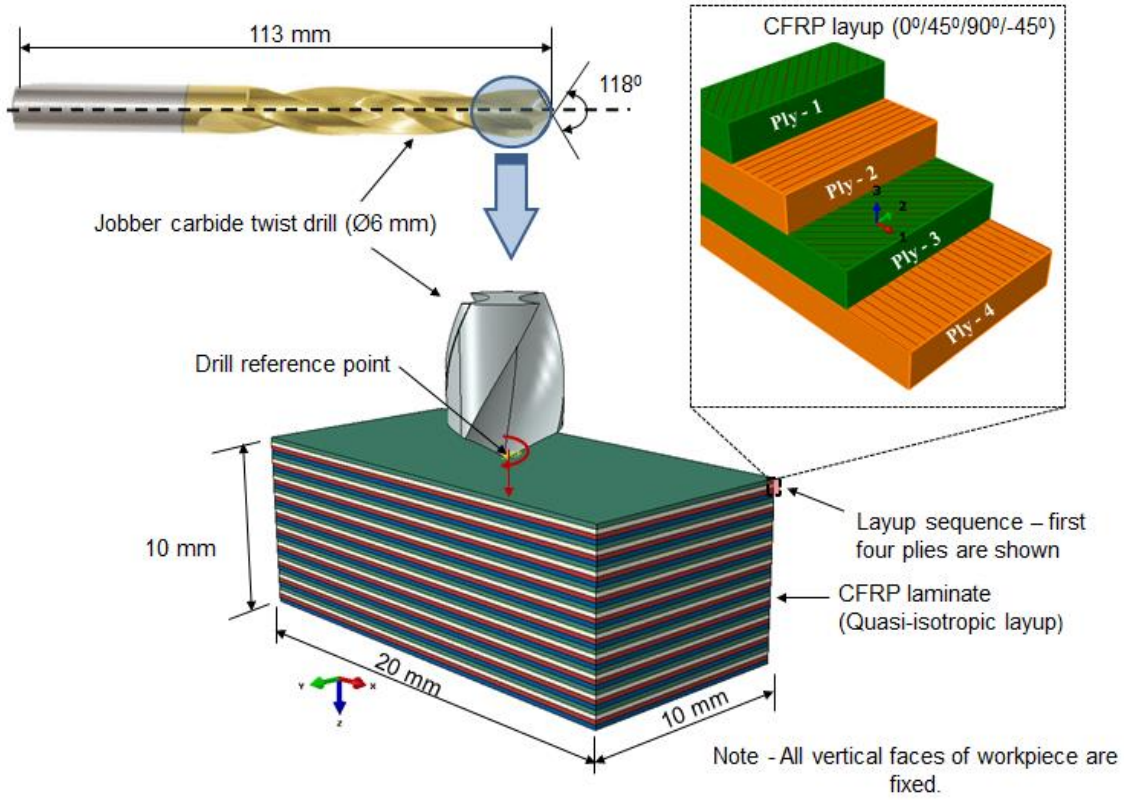



**Figure 3**. Finite-element model of UAD in M21/T700 composite laminate

The CFRP laminate was fixed at all four vertical faces, while the drill was constrained to rotate only about its own axis with a specified speed and fed vertically downwards into the work piece. The FE analysis was performed with experimentally optimised drilling parameters: spindle speed of 40 rpm, feed rate of 8 mm/min, vibration frequency of 27.8 kHz, peak-to-peak vibration amplitude of 12 μm. In order to incorporate the vibrating boundary condition, a time-dependent sinusoidal movement representing a cycle of ultrasonic vibration was imposed on the drill in the axial direction. Each wave consisted of 27,800 periodic sampling points for one second of simulated period of drilling. The drill

is thus vibrated along the vertical direction as well as rotated about its own axis independently.

*2.6.2. Choice of finite-elements*

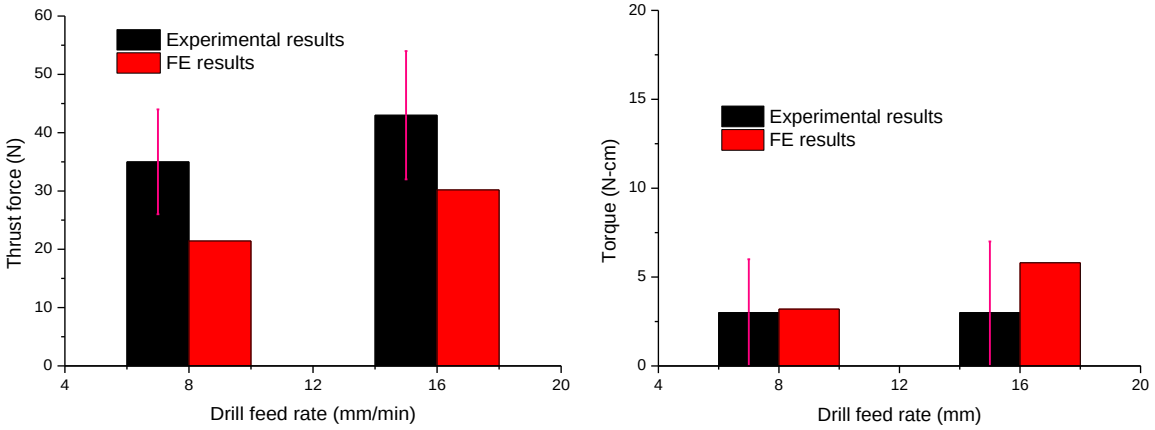
The Hill's potentential mainly depends on the deviatoric stress components and the plastic response becomes almost incompressible [16, 17]. Thus, finite-elements were chosen so that they could accommodate incompressibility, where plastic flow dominates the response. The fully integrated first-order continuum elements in Abaqus/Explicit were used with selectively reduced integration, whereby the volumetric strain was calculated at the centroid of the element only. In an adiabatic heat transfer analysis, the heat equation solved at each integration point is:

$$\rho c(\theta)\dot{\theta} = r^{pl} \quad , \tag{1.16}$$

where $r^{pl}$ the heat flux per unit volume due to plastic strain is, $\rho$ is the material density $c(\theta)$ is specific heat and $\dot{\theta}$ is the instantaneous temperature gradient. Since adiabatic heat is calculated using material properties and no external heat flux is added into the system, temperature degrees of freedom were not required. Hence eight-node, first-order, reduced-integration hexahedral elements of type C3D8R were used in this simulation. The CFRP model consisted of 820000 elements with the smallest element size of 5 μm. The drill was meshed with 35000 elements, with the smallest element size of 125 μm. The drill was modelled with four-node, 3D discrete rigid elements of type C3D4.

## 3. FE Results

The results obtained from FE simulations comprise the average of peak thrust force and torque for UAD in CFRP laminate. The thrust force and torque obtained under similar machining parameters and material properties with conventional drilling technique [5-7] are also presented for the comparison purpose and are shown in Fig. 4a and b.




(a) (b)

**Figure 4.** Comparison of peak thrust force (a) and peak torque (b) using experiments and FEA ($a = 12$ μm, $f = 27.8$ kHz )

## 4. Conclusions

A finite-element model of UAD in CFRP is developed using Abaqus 6.11. A constitutive material model suitable to model both volumetric and thermal softening in CFRP laminate under ultrasonic vibrations is proposed. The FE model replicated UAD process effectively. The FE results were found to be in good agreement with experimental findings. Additionally, the relative thrust force and torque reduction indicates good co-relation with the experimental results, demonstrating potential capabilities of the developed model to predict features of UAD.

**References**

[1] Rodriguez J P, Ashcroft I A and Silberschmidt V V 2008 *Compos. Sci. Technol.* **68** 2401-9
[2] Xia Z H and Curtin W A 2008 *Compos. Sci. Technol.* **68** 2526
[3] Lee C K 2009 *Mater. Chem. Phys.* **114** 125-33
[4] Zitoune R, Krishnaraj V, Almabouacif B S and Collombet F 2012 *Compos. Part B.* **43** 1480
[5] Makhdum F, Jennings L T, Roy A and Silberschmidt V V 2012 *J. Physics: Conf. Series.* **382** 12019
[6] Makhdum F, Nurdiya D K, Roy A and Silberschmidt V V 2012 *Solid State Phenom.* 188:170-5
[7] Phadnis V A, Makhdum F, Roy A and Silberschmidt V V 2012 *Proc. CIRP.* **1** 455-9
[8] Astashev V K and Babitsky V I 2007 *Ultrasonic processes and machines: dynamics, control and applications* (Berlin: Springer)
[9] Thomas P and Babitsky V I 2007 *J. Sound. Vib.* **308** 815
[10] Alam K, Mitrofanov A V and Silberschmidt V V 2011 *Med. Eng. Phys.* **33** 234
[11] Babitsky V I, Astashev V K and Meadows A 2007 J. *Sound Vib.* **308** 805-14
[12] Wiercigroch M, Wojewoda J and Krivtsov A 2005 *J. Sound Vib.* **280** 739-57
[13] Hocheng H, Taib N H and Liu C S 2000 *Compos. Part A*. **31** 133-42
[14] Wang X and Wang L 2004 *J. Mat. Process Tech.* **148** (2) 239-44
[15] Lucas M, MacBeath A and Cardoni E 2006 *Ultrasonics* **44** 503-509
[16] Hill R 1990 *J. Mech. Phys. Solids*. **38**(3) 405-17
[17] Hill R 1998 *The Mathematical Theory of Plasticity.* Clarendon Press
[18] Hillerborg A 1985 *Mat. Struct.* **18**(4) 291-6
[19] Abaqus 6.11 2011 *User manual* Dassault System Rhode Island US